

A submillimetre-selected, ultraluminous, active galaxy

R. J. Ivison,¹ Ian Smail,² J.-F. Le Borgne,³ A. W. Blain,⁴ J.-P. Kneib,³
J. Bézecourt,³ T. H. Kerr⁵ and J. K. Davies⁵

¹ *Institute for Astronomy, Dept. of Physics & Astronomy, University of Edinburgh, Blackford Hill, Edinburgh EH9 3HJ*

² *Department of Physics, University of Durham, South Road, Durham DH1 3LE*

³ *Observatoire Midi-Pyrénées, 14 Avenue E. Belin, F-31400 Toulouse, France*

⁴ *Cavendish Laboratory, Madingley Road, Cambridge CB3 0HE*

⁵ *Joint Astronomy Centre, 660 N. A'ohōkū Place, University Park, Hilo HI 96720, USA*

Accepted ... ; Received ... ; in original form ...

ABSTRACT

We present a detailed study of SMM02399–0136, an ultraluminous, active galaxy selected from a sub-mm survey of the distant Universe. This object is the brightest source in the fields of four rich, lensing clusters, with a total area of ~ 20 arcmin², that we have mapped with a sensitivity better than 2 mJy beam^{-1} at $850 \mu\text{m}$. We identify a compact optical counterpart with an apparent magnitude of $B \sim 23$ and a low-surface-brightness companion about 3 arcsec away. Our spectroscopy shows that components have the same redshift; $z = 2.803 \pm 0.003$. The narrow emission lines, $\text{FWHM} \simeq 1000\text{--}1500 \text{ km s}^{-1}$, and line ratios along with the compact morphology and high luminosity ($M_B \simeq -24.0$) of the galaxy indicate that SMM02399–0136 contains a rare dust-embedded, narrow-line or type-2 active galactic nucleus (AGN). The source is gravitationally lensed by the foreground cluster, amplifying its apparent luminosity by a factor of 2.5, and our detailed lens model allows us to correct robustly for this. Taking the amplification into account we estimate that SMM02399–0136 is intrinsically a factor of five times more luminous than *IRAS* F10214+4724. Its far-infrared and $\text{H}\alpha$ luminosities and low-surface-brightness radio emission all indicate an extremely high star-formation rate — several thousand solar masses per year — suggesting that SMM02399–0136 comprises an AGN buried in an interaction-induced starburst. A dust mass of $5\text{--}7 \times 10^8 M_\odot$ is indicated by our data for a dust temperature of 40–50 K, independent of whether the dominant energy source is an AGN or a starburst. We estimate the possible space density of such luminous sub-mm sources, and find that while a very large population of these obscured sources could be detected in future wide-field sub-mm surveys, they are unlikely to dominate the faint counts in this waveband. Galaxies like SMM02399–0136 and F10214+4724 cannot be easily detected in conventional AGN/QSO surveys, and so estimates of the prevalence of AGN in the early Universe may require significant revision.

Key words: galaxies: active – galaxies: starburst – galaxies: formation – galaxies: individual: SMM02399–0136 – cosmology: observations – cosmology: early universe

1 INTRODUCTION

There is abundant evidence that a large amount of dust exists in galaxies in the distant Universe. Many sub-mm detections of known high-redshift radio galaxies and quasars have been made following the identification of the ultraluminous *IRAS* source, F10214+4724, at $z = 2.286$ (Rowan-Robinson et al. 1991), for example: 4C41.17 (Dunlop et al. 1994), BR1202–0725 (Isaak et al. 1994) and 8C1435+635 (Ivison et al. 1998). These observations detect starlight, and/or quasar light, re-radiated by dust in the rest-frame far-IR

waveband. The discovery of F10214+4724 suggested that the *selection* of distant, star-forming sources in the sub-mm would become commonplace. This is still the perceived wisdom, although more recent work has provided a cautionary lesson by demonstrating that the extremely high luminosity of F10214+4724 is due to a strongly-lensed, dust-embedded AGN rather than solely to a starburst (e.g. Broadhurst & Lehar 1995; Eisenhardt et al. 1996; Goodrich et al. 1996; Serjeant et al. 1998).

Nevertheless, the sub-mm waveband still offers excellent prospects for the detection of a large population of very

distant, star-forming galaxies and, based on F 10214+4724, dusty AGN. The steep slope of the modified blackbody spectrum of dusty galaxies in the sub-mm and far-IR wavebands leads to large, negative K -corrections, which can even be sufficient to overcome the effects of the inverse square law (Blain & Longair 1993). A flat flux density-redshift relation is predicted for star-forming galaxies and dusty AGN at $z > 0.5$, and so the selection function of a sub-mm survey is expected to be relatively constant and to extend out to redshifts $z \sim 10$. This unusual selection function is expected to increase the detectability of lensed objects in sub-mm surveys (Blain 1996a, 1997a,b).

The first discovery of a population of objects in the sub-mm waveband has recently been made with the new Sub-mm Common-User Bolometer Array (SCUBA) on the 15-m James Clerk Maxwell Telescope (JCMT). Smail, Ivison & Blain (1997; SIB) took advantage of the gravitational amplification of the background sky seen through rich, lensing clusters to undertake the first, effectively blank-field, deep sub-mm survey. The sources detected in the fields of the rich cluster lenses, A 370 and Cl 2244–02, have allowed the sub-mm counts of distant galaxies to be measured for the first time, as compared with recent upper limits reported at other mm and sub-mm wavelengths by Phillips (1997) and Wilner & Wright (1997). Our dataset has now expanded to cover four independent fields (Blain, Smail & Ivison 1998), all mapped with a sensitivity better than 2 mJy beam^{-1} at $850 \mu\text{m}$. The cumulative $850 \mu\text{m}$ source counts at faint flux densities are substantially higher than those predicted by a simple non-evolving extrapolation of the local $60 \mu\text{m}$ galaxy luminosity function (Saunders et al. 1990). SIB concluded that the comoving star-formation density in the Universe associated with sources that have apparently very high star-formation rates, in excess of about $100 \text{ M}_{\odot} \text{ yr}^{-1}$, evolves strongly between $z = 0$ and $z > 1$ (also see Blain et al. 1998).

In view of the impact of the sub-mm surveys on our view of galaxy formation in the distant Universe, a more detailed study of the individual galaxies detected by SIB is clearly warranted. Here we present the results of follow-up observations of the brightest of these sub-mm sources, SMM 02399–0136, in the field of A 370. A similar analysis of the remaining sources will be presented in Ivison et al. (1998, in preparation). Here we have exploited the excellent archival data available for these rich clusters, as well as obtaining new data, in order to investigate the properties of SMM 02399–0136. First, we discuss the archival data; deep *UBVRI* images, ultra-deep 1.4 and 8.7 GHz radio maps and limits from *ROSAT* and *IRAS*. Secondly, we introduce the new observations; more sensitive SCUBA sub-mm maps and photometry, CFHT/UKIRT optical/near-IR imaging and spectroscopy and CAM imaging data from *ISO*. Thirdly, we discuss the nature of the source, and finally its implications for the interpretation of our sub-mm survey and the population of AGN in the distant universe. Throughout we assume $\Omega_0 = 1$ and $H_0 = 50 \text{ km s}^{-1} \text{ Mpc}^{-1}$.

2 OBSERVATIONS

SMM 02399–0136 is the brightest of the six sources detected in the $850 \mu\text{m}$ SCUBA maps of the distant rich clus-

ters, A 370 and Cl 2244–02 (SIB). It lies in the field of the $z = 0.37$ cluster, A 370, and is detected both in the $850 \mu\text{m}$ map at high significance (also appearing in the off-beams) and at a lower signal-to-noise ratio at $450 \mu\text{m}$ (Fig. 1). The original maps have now been augmented by a further 10 ks integration, giving a total integration time of 33.7 ks and an rms noise level of $1.5 \text{ mJy beam}^{-1}$ (Ivison et al. 1998, in preparation). The 33.7 ks maps can be used to deduce a position $\alpha = 02^{\text{h}}39^{\text{m}}51.97^{\text{s}}$, $\delta = -01^{\circ}35'59.6''$ (J2000) that is accurate to within about 4 arcsec. All the observations are summarized in Table 1.

2.1 Archival data

We targeted distant, massive clusters in our sub-mm observations primarily to exploit the gravitational lensing amplification of background sources. However, these targets are also richly endowed with archival data of excellent quality, covering the whole spectrum from the radio to the X-ray, and providing a wealth of additional information on our sub-mm detections.

2.1.1 VLA observations

A 370 has been studied extensively at radio wavelengths, both to understand the radio properties of member galaxies and in the hope of identifying lensed radio sources seen through the cluster core. We have used these observations to place limits to the intensity of the radio emission from SMM 02399–0136 and to better define its position.

The most useful radio observation for our purpose is a very deep 1.4 GHz A-configuration VLA map (Owen & Dwarakanath 1998, in preparation; Fig. 1), with a noise level of only $10 \mu\text{Jy beam}^{-1}$. This image clearly shows a weak, slightly extended source at $\alpha = 02^{\text{h}}39^{\text{m}}51.82^{\text{s}}$, $\delta = -01^{\circ}36'00.6''$ (J2000), well within the sub-mm positional uncertainty of SMM 02399–0136, and within 1 arcsec of a compact optical source (§2.1.2). After deconvolution with the synthesized beam, the emission region is found to be 7.9 arcsec by 2.2 arcsec in size, with a position angle of 71° , a maximum surface brightness of $221 \mu\text{Jy beam}^{-1}$ and an integrated flux density of $526 \pm 50 \mu\text{Jy}$. The 1.4 GHz flux density corresponds to a rest-frame 5.3 GHz power of about $2.6 \times 10^{23} \text{ W Hz}^{-1} \text{ sr}^{-1}$, just below the detection thresholds of deepest radio surveys; for example, the Leiden–Berkeley Deep Survey (Windhorst, van Heerde & Katgert 1984) has a selection limit of 0.6 mJy at 1.4 GHz. At higher frequencies, H. Liang has kindly inspected a deep 8.7 GHz D-configuration VLA continuum map (Liang 1997; Fig. 1) with a resolution of about 8 arcsec, and placed a 3σ limit of $57 \mu\text{Jy}$ to the 8.7 GHz flux density.

2.1.2 Optical imaging

A 370 has been studied extensively in the optical since the first giant gravitational arc was identified in its core by Soucail et al. (1987). Hence, we have been able to gather together a number of high-quality images. These include very deep *BRI* images taken using the 3.6-m Canada–France–Hawaii Telescope (CFHT) in superb conditions, with

Table 1. The observed properties of SMM 02399–0136 from the radio to the UV waveband. None of these quantities are corrected for the effects of gravitational lensing.

Property	Telescope	SMM 02399–0136		Comment
		L1	L2	
$\alpha(J2000)$		02 ^h 39 ^m 51.88 ^s	02 ^h 39 ^m 52.10 ^s	Position from <i>I</i> image, accurate to ± 1 arcsec.
$\delta(J2000)$		−01°35′58.0″	−01°35′57.2″	Position from <i>I</i> image, accurate to ± 1 arcsec.
Redshift		2.803 ± 0.003	2.799 ± 0.003	See Table 2.
Flux density at:				
450 μm	JCMT	$69 \pm 15 \text{ mJy}^\dagger$		Using new, deeper map.
850 μm	JCMT	$26 \pm 3 \text{ mJy}^\dagger$		Using new, deeper map.
1350 μm	JCMT	$5.7 \pm 1.0 \text{ mJy}^\dagger$		Photometry mode.
2000 μm	JCMT	$< 8.4 \text{ mJy}^\dagger$		3σ limit. Photometry mode.
12 μm	<i>IRAS</i>	$< 91 \text{ mJy}$		Estimate from nearby FSC sources.
25 μm	<i>IRAS</i>	$< 86 \text{ mJy}$		Estimate from nearby FSC sources.
60 μm	<i>IRAS</i>	$< 428 \text{ mJy}$		Estimate from nearby FSC sources.
100 μm	<i>IRAS</i>	$< 715 \text{ mJy}$		Estimate from nearby FSC sources.
15 μm	<i>ISO/CAM</i>	$1.2 \pm 0.4 \text{ mJy}^\dagger$		Metcalf et al. (1998).
3.4 cm	VLA (D)	$< 57 \mu\text{Jy}$		3σ limit, 8.7 GHz.
21.5 cm	VLA (A)	$526 \pm 50 \mu\text{Jy}$		1.4 GHz.
B_{tot}	CFHT	22.69 ± 0.03	23.73 ± 0.05	Total magnitude
U_{ap}	<i>HST</i>	25.17 ± 0.19	> 25.4	Aperture magnitude, 3σ limit for L2.
B_{ap}	CFHT	23.88 ± 0.04	25.26 ± 0.09	Aperture magnitude
V_{ap}	Danish 1.5-m	24.01 ± 0.04	25.62 ± 0.11	Aperture magnitude
R_{ap}	CFHT	22.60 ± 0.04	24.43 ± 0.11	Aperture magnitude
I_{ap}	CFHT	21.88 ± 0.05	23.92 ± 0.15	Aperture magnitude
K_{ap}	UKIRT	19.10 ± 0.11	21.83 ± 0.73	Aperture magnitude
0.1–2.0 keV	<i>ROSAT/HRI</i>	$< 10^{-14} \text{ erg s}^{-1} \text{ cm}^{-2}$		3σ limit.

[†] In a break from sub-mm/far-IR convention, errors include the uncertainty in calibration.

0.4 arcsec seeing in the *I*-band and 0.6 arcsec seeing in *B* and *R*; total integration times were 17.5 ks in *B* and 9.0 ks in both *R* and *I*. More information is given in Kneib et al. (1993, 1994). We also have a 18.0 ks integration in *V* with 1.3 arcsec seeing from the Danish 1.5-m telescope at La Silla, Chile (Smail et al. 1991).

A 370 has also been observed by the *Hubble Space Telescope* (*HST*) but, unfortunately, SMM 02399–0136 falls outside the field of view of the post-refurbishment WFPC2 observations by Saglia (GO 6003), and while the source is included in the pre-refurbishment WF/PC1 F702W (*R*-band) image of Dressler (GO 2373), discussed by Couch et al. (1994), this image lacks the surface brightness sensitivity necessary to provide detailed morphological information. SMM 02399–0136 was also included in a 16.4 ks WFPC2 F336W (*U*-band) image of Deharveng (GO 5709), which samples the rest-frame spectral energy distribution (SED) of the source at wavelengths between 830 and 930 Å. For aperture photometry with this data, we adopt the zero-point from Table 7 of Holtzman et al. (1995), and assume $(U - B) = 0$ to convert between the F336W and *U*-band magnitudes.

We find two faint optical sources within 3 arcsec of the 1.4 GHz position (§2.1.1): SMM 02399–0136[L1] and [L2] (Figs 1 & 2). L1 lies within 1 arcsec of the radio position, while L2 lies 3 arcsec to the East, at a position angle of about 88°. Two other considerably fainter sources are visible in the *I*-band image to the N and NNE within 2 arcsec of L1;

however, because of their faintness and the coarser angular resolution of our other optical images, these features are not visible in the other bands, and so we concentrate on L1 and L2 below. The results of aperture photometry in 1.5 arcsec diameter apertures from the seeing-matched *UBVRIK* images are listed in Table 1, along with estimates of the total *B*-band magnitude of each component. The reddening towards A 370 is $E(B - V) = 0.015$, and so no foreground reddening correction has been applied to the results in Table 1.

L1 is brighter than L2 in our high-resolution *I*-band image (Fig. 2; Table 1). It appears to have a compact morphology, and is marginally resolved with an intrinsic FWHM of 0.3 arcsec. The WF/PC1 F702W and WFPC2 F336W images show an unresolved source, with a FWHM of about 0.1–0.2 arcsec, coincident with L1. The F336W exposure also shows some emission associated with L2. From our ground-based images we can see that L2 has a diffuse morphology with a profile which extends out to L1 (Fig. 2). Source morphologies are discussed in more detail in §3.2.

2.1.3 Observations in other wavebands

A deep *ROSAT* High Resolution Imager exposure of A 370 with a total exposure time of 30.8 ks, taken by Böhringer, was retrieved from the *ROSAT* HEASARC Archive at GSFC. The positional accuracy is good to within about 8 arcsec, based on the relative positions of bright stars and

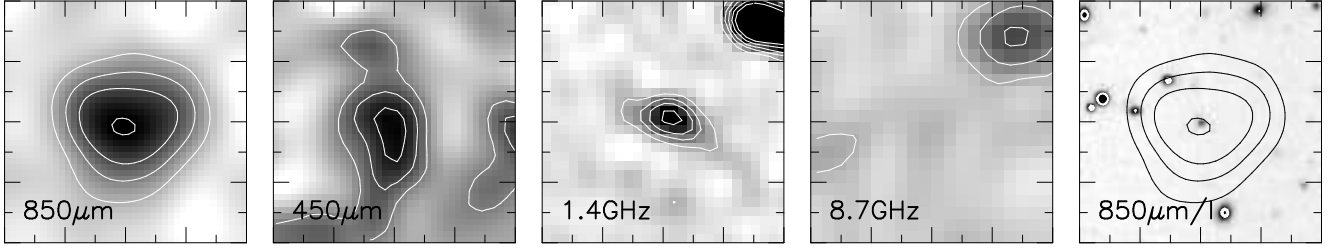


Figure 1. Maps of SMM02399–0136. From left to right: 850 μm SCUBA image; 450 μm SCUBA image; 1.4 GHz VLA A-configuration map; 8.7 GHz VLA D-configuration map; and the 850 μm SCUBA map overlaid on a CFHT *I*-band image. North is up and East is to the left. Each panel is 40 arcsec square.

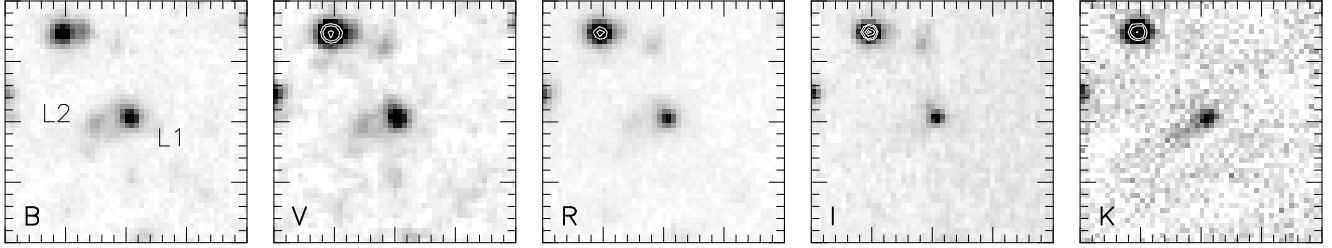


Figure 2. *BVRIC* images of SMM02399–0136. The two optical counterparts, L1 and L2, are identified in the *B*-band exposure; both have red colours across these passbands. Note that L1 appears very compact in all passbands, even at the very fine 0.4–0.6 arcsec resolution of the CFHT *BRI* exposures. The low-surface-brightness feature L2 may be either a companion or the remnant of a tidal interaction that triggered the activity in L1. North is up and East is to the left. Each panel is 20 arcsec square.

galaxies in this exposure and our wide-field optical images. Due to the extended emission from the hot intracluster gas in the foreground cluster, it is difficult to identify any obvious emission from SMM02399–0136. By fitting and subtracting a smooth background we estimate a 3σ upper limit of $S_\nu \lesssim 10^{-14} \text{ ergs}^{-1} \text{ cm}^{-2}$ to the flux in the 0.1–2 keV band from a point source at this position in a 24 arcsec aperture. Assuming $S_\nu \propto \nu^{+\alpha}$, with $\alpha \simeq -0.5$ for an obscured source (Almaini et al. 1995), and a Galactic HI column density of about $3 \times 10^{20} \text{ cm}^{-2}$, this flux density corresponds to a luminosity of less than $5 \times 10^{44} \text{ ergs}^{-1}$ in the 2–10 keV band at $z = 2.8$ (§2.2.2), after correcting for lens amplification, which is consistent with a type-2 AGN (c.f. Lawrence et al. 1994).

The relatively uninteresting *IRAS* All-Sky Survey upper limits at 12, 25, 60 and 100 μm are listed in Table 1.

2.2 New targeted observations

2.2.1 New measurements with SCUBA on the JCMT

Follow-up observations with SCUBA have been made using the photometry mode at 1.35 and 2 mm. As reported by SIB, the secondary mirror was chopped at 6.944 Hz, but instead of the previous, complex jiggle pattern, a simple ‘filled-square’ 9-point jiggle was performed with 2 arcsec offsets in both the signal and reference beams, nodding between the two every 18 s in a signal–reference–reference–signal pattern. Every hour the pointing was checked on the blazar 0336–019 and a skydip was performed to measure the atmospheric opacity. The rms pointing errors were about 2 arcsec.

The data was reduced by carefully rejecting spikes and then subtracting the measurements in the reference beam from those in the signal beam. The data was then corrected

for atmospheric opacity and calibrated against Uranus. The measured flux densities, and those derived from the deeper 450 and 850 μm maps discussed earlier in §2, are listed in Table 1.

2.2.2 Optical spectroscopy from CFHT

Initial spectroscopy of SMM02399–0136 was undertaken with the MOS multi-object spectrograph on the 3.6-m CFHT, Mauna Kea, on the nights of 1997 Sept 5–7. The (2k)² SiTe CCD was used with the O300 grism and slitlets 15 arcsec in length and 1.2 arcsec in width, which were aligned along the line joining L1 and L2 (a position angle of 88.6°). A number of both sub-mm- and optically-selected sources were targeted across the field of A370. The mask containing SMM02399–0136 was observed for a total of 24.3 ks, in nine 2.7 ks exposures. The data were debiased and flatfielded using dome flats in the standard manner, and then the one-dimensional spectra of both L1 and L2 were optimally extracted. The spectra were calibrated in wavelength using He–Ar arc spectra that were interspersed between the science exposures, and in flux density using observations of Feige 110 (Oke 1990). The final spectra (Fig. 3) cover the wavelength range 3500–10000 Å at high sensitivity, with 4.7 Å pixel^{-1} sampling and an effective resolution of about 15 Å at 4500 Å; the wavelength calibration is accurate to within 0.1 Å rms. At wavelengths longer than 7500 Å the data are contaminated by the second-order spectra, and so these wavelengths are not shown in Fig. 3. To demonstrate the spatial separation of L1 and L2, and to highlight their different emission characteristics, a section of the two-dimensional spectrum around the Ly α line is shown in Fig. 4.

A number of narrow emission lines and absorption features superimposed on a blue continuum can be identi-

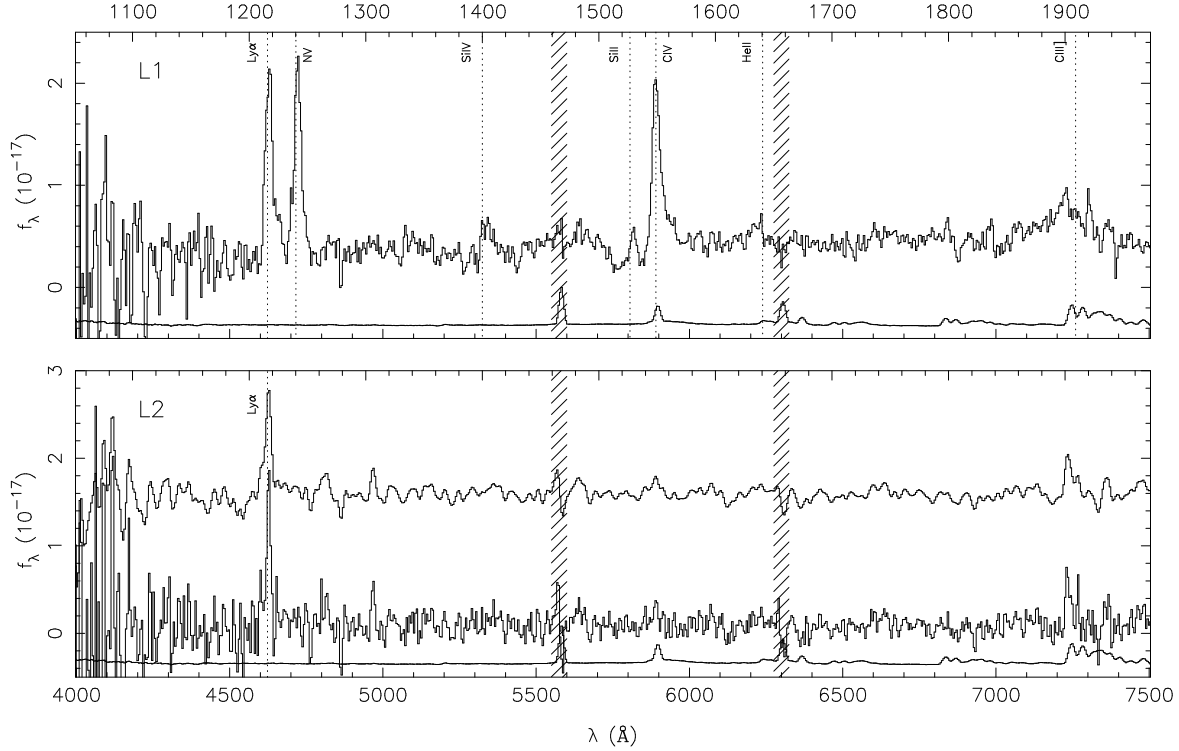


Figure 3. Optical spectra of both L1 and L2 from the MOS spectrograph on CFHT. The spectrum of L1 shows a number of narrow emission lines at $z = 2.803$ superimposed on a blue continuum, with hints of broad absorption features on the blue wings of some lines. The spectrum of the substantially fainter L2 shows only $\text{Ly}\alpha$ at a similar redshift to that of L1. The lower spectrum in each panel is an arbitrarily scaled sky spectrum, which indicates the positions of sky emission features; the hatched regions are strongly affected. The identified optical lines listed in Table 2 are indicated. The observed wavelength is shown on the bottom axis: the rest-frame wavelength at $z = 2.8$ is shown on the top axis. The spectra of L1 and L2 are flux calibrated and are plotted in units of $10^{-17} \text{ erg cm}^{-2} \text{ s}^{-1} \text{ \AA}^{-1}$.

fied in the spectrum of L1 (Table 2), the most prominent of these lines are redshifted $\text{Ly}\alpha$ 1215.7Å, N v 1240.2Å and C iv 1549.0Å. Using all the features listed in Table 2, we estimate a redshift $z = 2.803 \pm 0.003$, at which an angular scale of 1 arcsec corresponds to 7.45 kpc. The FWHM of these emission lines are typically about 26Å, which is equivalent to about 1000–1500 km s^{-1} in the rest frame after correcting for the instrumental broadening (Table 2). We see no evidence for a broad component of these lines, although some are slightly asymmetric. This asymmetry may be related to blue absorption troughs, the most prominent of which are associated with C iv/Si II and Si IV . The typical width of these troughs is about 70–150Å, corresponding to about 3000–7000 km s^{-1} at $z = 2.8$. We do see one broad line in the spectrum of L1 at 7000–7400Å, although this lies on an atmospheric OH bandhead. We identify this feature as broad $\text{C III}]$ 1909Å, with an apparent FWHM of about 180Å, or around 7400 km s^{-1} in the rest frame (c.f. Serjeant et al. 1998; although see Hartig & Baldwin 1986 for other possible identifications). The only feature of interest outside the wavelength range shown in Fig. 3 is a possible detection of a very weak $\text{Ly}\beta$ line at a rest-frame wavelength of 1026Å. These features are discussed in more detail in §3.3.

The only strong line detected in the spectrum of the fainter, diffuse source, L2, is $\text{Ly}\alpha$ 1215.7Å at a similar wavelength to that observed in L1; there is little or no continuum (Figs 3 & 4). The deconvolved velocity width of the $\text{Ly}\alpha$ line is about 500 km s^{-1} , much narrower than the equivalent line

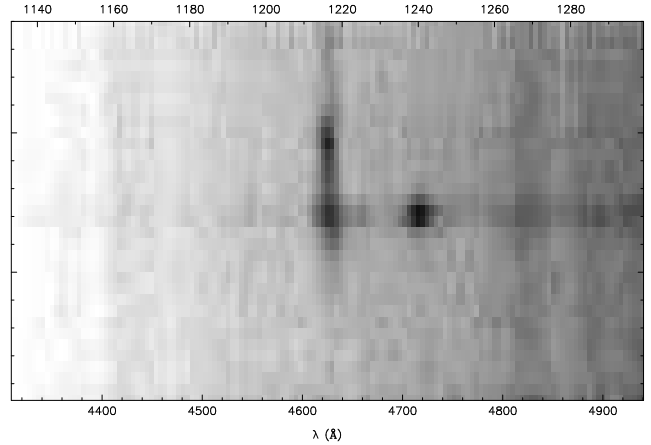


Figure 4. The two-dimensional optical spectrum of L1/L2 around the wavelength of the redshifted $\text{Ly}\alpha$ line. L1 is the lower of the two objects, a compact source with strong $\text{Ly}\alpha$ and N v emission lines; in contrast, L2 is clearly extended and shows only narrow $\text{Ly}\alpha$ emission. The observed and rest-frame wavelengths are shown on the bottom and top axes respectively; the tick marks on the vertical axis are separated by 1 arcsec.

in L1 (Table 2). Looking at Fig. 4 we see that the $\text{Ly}\alpha$ emission extends beyond the peak in L2 out to a distance of at least 8 arcsec from L1, beyond the continuum extent of the source shown in Fig. 2.

Table 2. Spectral line identifications in SMM 02399–0136 [L1] and [L2]. λ_{obs} is the observed wavelength, λ_0 is the emitted wavelength if the redshift of the line is z .

Line	λ_{obs} (Å)	λ_0 (Å)	z	EW (Å)	FWHM (km s ⁻¹)	Comments
L1						
Ly α	4623.90	1215.7	2.804	−195.3	1850	Red wing.
N v	4717.53	1240.2	2.804	−167.1	1790	Red wing.
Si IV + O IV]	5335.00	~1400	$\simeq 2.8$	−23.4	1790	Absorption trough to blue.
Si II	5813.05	1526.7	2.808	−33.7	1160	Possible absorption trough to blue, lies in CIV trough.
C IV	5887.76	1549.0	2.801	−111.7	1560	Red wing, absorption trough to blue.
He II	6222.19	1640.5	2.793	−19.6	2800	
C III]	7220.84	1908.7	2.783	−156.2	7700	Very broad feature on OH band head.
[O III]	18991	5006.9	$\simeq 2.8$...	1020	$\sim 8 \times 10^{-18} \text{ W m}^{-2}$.
H α /[N II]	$\simeq 24881$	6548/6563	$\simeq 2.8$...	1060	$\sim 9 \times 10^{-18} \text{ W m}^{-2}$.
L2						
Ly α	4622.96	1215.7	2.803	−250	900	
[O III]	19050	5006.9	2.805	...	1600	$\sim 2 \times 10^{-17} \text{ W m}^{-2}$.
H α /[N II]	$\simeq 24905$	6548/6563	$\simeq 2.8$...	680	$\sim 5 \times 10^{-18} \text{ W m}^{-2}$.

2.2.3 Infrared imaging and spectroscopy with UKIRT

During 1997 July 18, we obtained a *K*-band image of the A 370 field using the IRCAM3 near-IR camera on the 3.8-m UK Infrared Telescope (UKIRT) in 1.0 arcsec seeing (T. Naylor, private communication). The measurements were made in blocks of nine 60 s sub-exposures, the first centred on SMM 02399–0136 and the following eight offset by 8 arcsec. Eight repetitions gave a total integration time of 4.3 ks. The resulting image is shown in Fig. 2: L1 and an extension in the direction of L2 are clearly visible. Photometry from this image is listed in Table 1.

A *K*-band spectrum was obtained using the CGS4 spectrometer on UKIRT during 1997 Oct 5 in good conditions and 0.7 arcsec seeing. The 40 lines mm⁻¹ grating was used to cover the entire *K*-band window at a resolution of 560 km s⁻¹. A 90 arcsec-long, 1.22 arcsec-wide slit was used at a position angle of 88°, the data were Nyquist sampled and the telescope was nodded 18.3 arcsec along the slit every 80 s to allow adequate sky subtraction. Offsets from a nearby bright star were used to position the slit accurately on the object. The total exposure time was 4.6 ks. Flux calibration and telluric line cancellation were performed by ratioing the spectrum with that of CMC 100796, a F0V star, and then multiplying by a blackbody spectrum appropriate to the temperature and magnitude of that star.

Continuum emission can be discerned in the spectrum of L1. The [O III] 4959 and 5007 Å lines are present at a 4 σ significance, blended together at the blue end of the spectrum, corresponding to $z \simeq 2.793$. They are blueshifted slightly with respect to the optical emission line, although there are no arc lines near this wavelength, and so the uncertainty in the wavelength calibration is increased. The flux density in the [O III] 5007 Å line is about $8 \times 10^{-18} \text{ W m}^{-2}$. Another line is also present at the extreme red end of the spectrum at 3 σ significance. Its wavelength is consistent with either pure H α 6563 Å or a blend of H α and [N II] 6548 Å. The flux density in the 1060 km s⁻¹ wide line is

about $9 \times 10^{-18} \text{ W m}^{-2}$. If it is H α , then the redshift is $z = 2.795 \pm 0.009$.

The [O III] 5007 Å line is clearly detected in the spectrum of L2 at 5 σ significance, with [O III] 4959 Å blended into its blue wing. A twin Gaussian profile, in which one component is three times brighter than the other but with an identical width, fits the profile very accurately at the expected wavelength ratio and $z \simeq 2.805$, although again the wavelength calibration may be slightly uncertain. The H α or H α /[N II] blend seen towards L1 is also present in the spectrum of L2, but only at the 2 σ level, corresponding to a flux density of about $5 \times 10^{-18} \text{ W m}^{-2}$.

2.2.4 Mid-infrared data from ISO

During 1996 Aug 18–19, Metcalfe et al. (1998) obtained an extremely deep mid-IR image of A 370, targeting the giant arc, A0, with the long-wavelength channel of the 32²-pixel camera ISOCAM (Césarsky et al. 1996) using a 2.75 μm -wide filter centred at a wavelength of 15 μm . The total integration time near SMM 02399–0136 was 1.6 ks, and the source was detected at a significance of about 40 σ , although not resolved. The 15 μm flux density is $1.2 \pm 0.4 \text{ mJy}$ after accounting for the uncertainty in calibration (L. Metcalfe, private communication).

3 RESULTS

3.1 Gravitational lensing

Before discussing the detailed continuum and spectral-line properties of SMM 02399–0136, it is important to clarify the degree of amplification experienced due to the massive, concentrated, foreground cluster. Detailed mass models (Kneib et al. 1993; Bézecourt et al. 1998, in preparation) suggest that the for a $z = 2.8$ source at this position in the lens the most likely amplification factor is 2.5, with a robust upper

limit of 5. A factor of 2.5 is assumed below, and this correction will always have been applied to the derived physical quantities, for example M_B and dust mass.

3.2 Morphology

The UV and optical images (Fig. 2) indicate that SMM 02399–0136 has two related counterparts, L1 and L2. L1, the compact component, may be marginally resolved with an intrinsic FWHM of 0.3 arcsec, corresponding to about 1 kpc in our adopted cosmology at $z = 2.8$ after correcting for lens amplification. The angular separation of L1 and the brightness peak in L2 is about 3 arcsec, corresponding to 22 kpc, or ~ 9 kpc after correcting for amplification in the tangential direction, this is roughly along the line joining L1 and L2. L2 has a more complex morphology than L1, showing a ridge of emission to the North and a relatively diffuse region extending South and West towards L1.

The radio emission from the 1.4 GHz maps is also resolved in the East-West direction, with the low-surface-brightness emission extending out 8 arcsec, or ~ 24 kpc after correcting for lensing. This is evidence that the radio emission may be fueled by supernova activity related to an extended starburst region, rather than by an AGN, although the relative contributions of L1 and L2 cannot be determined reliably. The extent of the radio source corresponds approximately to that of the Ly α emission region (Fig. 4).

The structure seen within L2 and the AGN-like activity of L1 discussed below are consistent with L2 being a remnant or tidal debris associated with an interaction that triggered the activity in L1.

3.3 Spectral classification

The optical spectrum of L1 in Fig. 3 shows a wide range of high-ionization emission lines that are typical of both AGN and starburst galaxies. The most striking feature is the narrow rest-frame width of the lines, typically $\lesssim 1000$ – 1500 km s^{-1} (Table 2); Ly α and N V are well separated, as are C IV and He II. The line profiles are only very slightly asymmetric (Fig. 3), and the strongest lines show hints of red wings. Both of these features suggest that the narrow line widths are not caused by absorption in material outflowing from the source. If this was the case, then significant broad absorption lines (BALs) would be visible on the blue side of the lines. Weak BAL troughs are visible on the C IV, Si II and Si IV lines, and outflow velocities of about 5000 km s^{-1} are indicated.

With the exception of the broad, semi-forbidden C III] 1909 Å line, the narrowness of the emission lines and the presence of high-ionization lines, such as N V and C IV, indicates that the source is best classified either as a very luminous Seyfert II or as one of the rare class of narrow-line or type-2 QSOs (Baldwin et al. 1988), with weak BAL features. Using the definition of Heckman et al. (1995), based on the ratio of the strengths of the C IV and He II lines, the source would probably be placed in the narrow-line QSO class.

However, a detailed classification of L1 is probably unwarranted, especially given the presence of both narrow permitted and broad semi-permitted lines in a single source.

For our purposes it is enough to know that the characteristics of both Seyfert II and narrow-line QSOs are believed to arise from a dusty AGN, with a combination of emission from a slightly obscured narrow-line region and a highly obscured broad-line region. In the permitted lines, emission from the narrow-line region dominates, exhibiting a range of high-excitation line emission, with FWHM $\sim 1000 \text{ km s}^{-1}$. In the case of L1, the narrow-line region is seen through a weak BAL outflow. Some light does escape from the broad-line region and is seen in the semi-forbidden lines, such as C III] 1909 Å which exhibits a broad component. Hard X-rays may also escape (Ohta et al. 1996). The absence of a strong broad component to the H α line in L1 indicates that the reddening to the broad-line region of this object, A_V , probably exceeds about 8–10.

The spectrum of L1 shares many of the same properties shown in the well-studied *IRAS* source F 10214+4724 (e.g. Serjeant et al. 1998), which has been variously described as a proto-galaxy, starburst or Seyfert II. Both SMM 02399–0136 and F 10214+4724 show predominantly narrow emission lines, with broad C III] 1909 Å and low ratios of Ly α to N V (Serjeant et al. 1998).

Turning to the spectrum of L2, we see a stronger Ly α compared to the continuum, than in L1; also, N V, C IV and He II are absent. The morphology of L2 is suggestive of an interaction or merger between L1 and a companion, rather than as extended QSO ‘fuzz’ (e.g. Hutchings 1995). There are, however, spectral similarities between L2 with the extended emission-line regions associated with radio-loud quasars (e.g., Lehnert & Becker 1998); it is interesting to speculate that since the tangential amplification experienced by L2 leads us to postulate that it is the remnant of a merger, perhaps many examples of ‘fuzz’ have similar origins.

3.4 Spectral energy distribution

The radio–UV SED of L1 deduced from our observations is shown in Fig. 5. At wavelengths longer than about $10 \mu\text{m}$ this is effectively the SED of both L1 and L2. We have chosen not to confuse Fig. 5 by plotting the UV–optical data for L2. The SEDs of other far-IR luminous galaxies are also shown in Fig. 5. Comparing the far-IR luminosity of SMM 02399–0136 with that of F 10214+4724 (corrected for a lens amplification of 30) in Fig. 5, we see that SMM 02399–0136 is roughly five times more luminous, although such comparisons are sensitive to the exact amplification suffered by the emission regions in F 10214+4724 probed at these wavelengths, which is highly uncertain (Broadhurst & Lehar 1995). The closest match to SMM 02399–0136 in the UV and optical wavebands is with 8C 1435+635, a dusty radio galaxy — and presumably a massive elliptical — at $z = 4.25$. 8C 1435+635 also provides the best match to the SED in the far-IR waveband, but its radio luminosity far exceeds that of SMM 02399–0136. We briefly discuss the properties of the source across the wavelength range shown in Fig. 5, starting at the shortest wavelengths.

Both L1 and L2 have a smooth, steep UV–optical–mid-IR continuum and blue optical and near-IR colours. The exception being the red ($U - B$) colour caused by the presence of the redshifted Lyman-limit in the F336W passband.

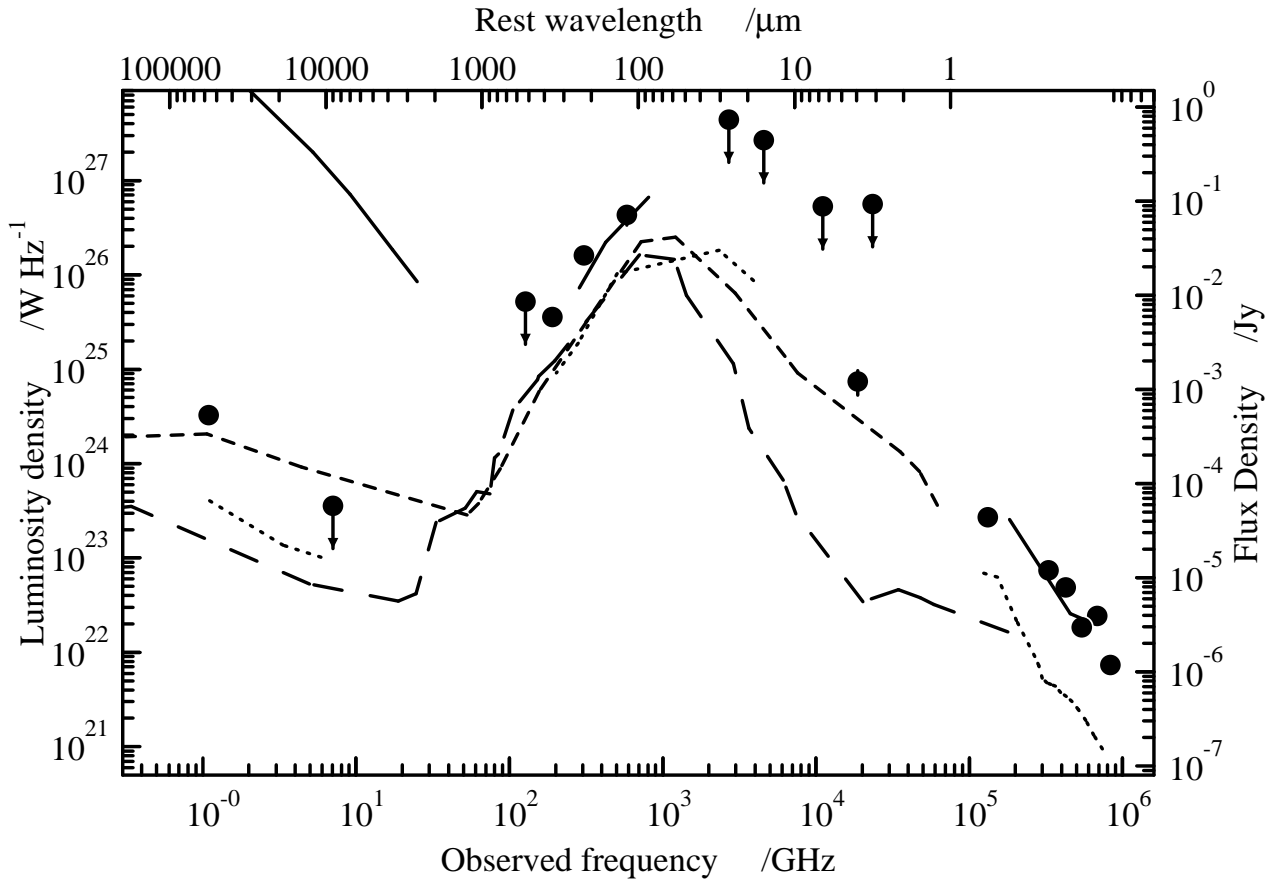


Figure 5. The SED of SMM 02399–0136 between the radio and optical wavebands, represented by filled circles. The right-hand scale gives the flux densities for this source. For comparison, we have plotted the SEDs of the ultraluminous *IRAS* sources F 10214+4724 (dots), Mrk 231 (dashes) and Arp 220 (long dashes) and the radio galaxy 8C 1435+635 (solid), with units of luminosity density (left-hand scale). These lines are broken in regions where only upper limits to the SEDs are available. The SEDs were taken from Rowan-Robinson et al. (1993), Barvainis et al. (1995), Ivison et al. (1997, 1998) and D.H. Hughes (private communication); for F 10214+4724 and SMM 02399–0136 they are corrected for lensing by factors of 30 and 2.5 respectively.

L2 is slightly bluer than L1, the UV–optical spectral index, α , where $S_\nu \propto \nu^{+\alpha}$, is in the range -1.5 to -1.9 for L1 — much steeper than that seen in most unobscured QSOs, and closer to $\alpha \simeq -1.1$ for L2. The distance modulus at $z = 2.8$ is 47.64, and so L1 has a K -corrected absolute magnitude $M_B = -24.0$ for a UV–IR spectral index, $\alpha = -1.65$, while L2 has $M_B = -22.1$ (with $\alpha \simeq -1.1$). Across the rest-frame UV–IR spectral index we find a similarly steep spectrum with $\alpha = -1.65$ for the composite source L1/L2, although the SED is poorly constrained at wavelengths between about 25 and 50 μm . Future *ISO* observations probing these wavelengths will be crucial for the accurate determination of the temperature and optical depth of the dust that clearly dominates the SED at longer wavelengths.

In the far-IR, at rest-frame wavelengths between 120 and 350 μm , observed by SCUBA, the SED has the characteristic spectral index $\alpha \simeq +3$ of optically-thin emission from dust grains. Simple fits suggest that the dust temperature $T_d \simeq 40$ –50 K, although higher temperatures can be fit if the opacity of the dust becomes significant at wavelengths of about 100–200 μm . The luminosity in the far-IR waveband between observed wavelengths of 20 and 1000 μm , L_{FIR} , is about $10^{13} L_\odot$ if $T_d = 40$ K, and several times larger if either the dust opacity is significant or if T_d exceeds 40 K. Adopting $k_d = 0.15[\lambda_0/800 \mu\text{m}]^{-1.5}$ for the standard dust

emission parameter in order to facilitate comparisons with other distant objects (c.f. Ivison et al. 1998), where λ_0 is the rest-frame wavelength, we predict dust masses $M_d = 7 \times 10^8$ and $5 \times 10^8 M_\odot$, for $T_d = 40$ and 50 K respectively.

If the dust in SMM 02399–0136 is heated primarily by hot, young OB-type stars then the far-IR luminosity corresponds to a formation rate of stars with masses larger than $10 M_\odot$ of about $2000 M_\odot \text{ yr}^{-1}$, and to a total star-formation rate (SFR) of about $6000 M_\odot \text{ yr}^{-1}$ if the initial mass function (IMF) extends down to much lower masses (Thronson & Telesco 1986). A similarly high estimate of the SFR is given by the $H\alpha$ luminosity from our K -band spectrum. After correcting for lensing, but not for possible extinction, the combined $H\alpha$ luminosity of L1 and L2, $L_{H\alpha}$, is $\simeq 5 \times 10^{37} \text{ W}$, and so the total SFR is expected to lie in the range 2000–20000 $M_\odot \text{ yr}^{-1}$ (where the range includes the uncertainty in the relation derived by different authors — for example: Barbaro & Poggianti 1997; Kennicutt 1983; Hill et al. 1994). By any standards this is a spectacular starburst.

At still longer wavelengths, the 8.7 and 1.4 GHz measurements yield a steep index, $\alpha \lesssim -1.2$, which is typical for an optically-thin synchrotron source. It is steeper than the index measured in ultraluminous *IRAS* galaxies such as Arp 220, Mrk 231 and F 10214+4724 — for F 10214+4724, $\alpha = -0.9$ (Rowan-Robinson et al. 1993) — and may well be

as steep as the integrated emission from the radio galaxy, 8C 1435+635. The steep spectrum may be the signature of AGN-related emission: a dense interstellar medium can frustrate the formation of conventional lobes, causing the magnetic field to be advected up the jet. However, several scenarios involving star formation can equally explain the steep radio spectrum: either ongoing star formation, where cosmic-ray electrons with the highest energies are quickly lost to regions where the magnetic field is low; or a recent cessation of star formation which produces an absence of newly accelerated electrons. Furthermore, 2–10 per cent of the radio emission from spiral disks and nuclear starbursts is due directly to supernova remnants (SNRs), the dominant contribution being provided by cosmic rays (D’Odorico, Goss & Dopita 1982; Helou et al. 1985). There is no difficulty, therefore, in reconciling the observed radio emission with that expected from an intense starburst: first, the extended radio morphology is consistent with a starburst in L1, or both L1 and L2, rather than emission from a compact AGN; and secondly, the total SFR of greater than $1000 \text{ M}_{\odot} \text{ yr}^{-1}$, derived from L_{FIR} and $L_{\text{H}\alpha}$, is consistent with the supernova rate of $80\text{--}400 \text{ yr}^{-1}$ indicated by the radio emission, especially if the IMF is top heavy.

Due to the modest resolution of our sub-mm/radio maps we are unable to determine the relative contributions of L1 and L2 to the emission in these wavebands; however, the extended 1.4 GHz radio emission is roughly aligned with the orientation of L1/L2 and so at least part, and perhaps up to half, of the emission might be expected to originate in L2. If this is the case, and if the sub-mm dust emission has a similar distribution on small scales, then L2 might be the first non-active, sub-mm-selected high-redshift galaxy, and so the best candidate for a ‘primeval’ galaxy. Sub-mm observations at higher angular resolution will be crucial for better understanding the nature of such sources. The forthcoming generation of very sensitive large mm/sub-mm interferometers (Brown 1996; Downes 1996) will be especially effective in advancing these studies.

4 DISCUSSION

We have presented detailed follow-up observations of the brightest of six sub-mm-selected objects detected by Smail, Ivison & Blain (1997). These reveal a radio-quiet, active galaxy at $z = 2.8$ with a total bolometric luminosity of $\gtrsim 10^{13} L_{\odot}$. The $\text{H}\alpha$ emission from this source and its SED in the radio and far-IR wavebands are consistent with an SFR of several $1000 \text{ M}_{\odot} \text{ yr}^{-1}$. Its optical/UV spectrum is most consistent with that of a narrow-line, dust-obscured AGN, very similar to F 10214+4724. It is likely that both star formation and an active nucleus are each partly responsible for the high luminosity of SMM 02399–0136 as they appear to be in F 10214+4724 (Serjeant et al. 1998).

It is interesting to compare the properties of this source with the characteristics of the population of optically-selected AGN and to consider the consequences of this detection for future sub-mm surveys. In four fields surveyed to date we can place a limit of $250_{-220}^{+330} \text{ deg}^{-2}$ to the surface density of obscured AGN/starburst galaxies as luminous as SMM 02399–0136 at 90 per cent confidence, if we assume that the mean amplification factor is about 1.3 in

these fields and that the population of background sources is unclustered. This density is a factor of ~ 1.6 times larger than the surface density of optically-selected QSOs brighter than $B = 22$ (Bershady et al. 1998), and is comparable to the surface density of faint radio galaxies at flux densities of 0.2 mJy in the deepest 1.4 GHz surveys (Oort 1987). The magnitude and radio flux density limits given here are similar to the properties of SMM 02399–0136 after correction for lensing. Thus our observations of SMM 02399–0136 are consistent a population of distant, obscured AGNs with a surface density comparable to that of optically-selected quasars. Classical search techniques in the radio and optical wavebands are relatively insensitive to radio-quiet, dust-shrouded sources such as SMM 02399–0136, and so conclusions about the abundance and evolution of active galaxies at high redshifts that are based upon such approaches may have to be reassessed. Clearly extensive sub-mm surveys are needed to determine the actual abundance of such sources.

A population of highly obscured AGN might also provide a significant contribution to the diffuse X-ray background (XRB, Georgantopoulos et al. 1996). A population of galaxies similar to SMM 02399–0136 with a surface density of 250 deg^{-2} , each with a flux density close to our lensing-corrected 3σ upper limit of $4 \times 10^{-15} \text{ erg s}^{-1} \text{ cm}^{-2}$ at $0.1\text{--}2.0 \text{ keV}$ and a spectral index $\alpha \sim -0.5$ (Almaini et al. 1995) could contribute up to about 40 per cent of the total spectral intensity of the XRB at energies close to 1 keV , about $2.3 \times 10^{-12} \text{ keV cm}^{-2} \text{ s}^{-1} \text{ sr}^{-1} \text{ keV}^{-1}$ (Georgantopoulos et al. 1996). Such highly obscured sources have been proposed as the origin of the XRB owing to their flat spectral shape (Almaini, Fabian & Barcons 1998).

SIB carried out the first deep survey in the sub-mm waveband, and detected six sources. Here, we have shown that the brightest of these sources is an active galaxy. What are the consequences for both the conclusions drawn about the evolution of galaxies by SIB, and the prospects for future surveys based on this result? The preliminary analysis of SIB assumed that the energy source in all six detected galaxies was star formation. Clearly, at least a part of the luminosity of SMM 02399–0136 is produced by an active nucleus, and we have no further information about our other five detections. In general, an AGN source will have no effect on the predicted counts or intensity of background radiation in the sub-mm, but the rate of production of heavy elements in high-mass stars that is required to power these sources will be slightly reduced, it would still remain in agreement with current observations. Hence, the significant conclusions of SIB remain unchanged at present. If the other sources in the sample are also found to be active then this conclusion could change, although we feel this is unlikely.

Larger blank-field surveys in the sub-mm waveband are underway, and so an expanded sample of sources such as SMM 02399–0136 should soon be compiled (Blain & Longair 1996; Pearson & Rowan-Robinson 1996). In particular, ESA’s 3.5-m *Far-Infrared and Submillimetre Space Telescope (FIRST)* mission (Pilbratt 1997) is expected to survey an area of about 0.01 deg^2 at $480 \mu\text{m}$ with 35 arcsec resolution to a 1σ sensitivity of around 0.8 mJy in a 1 hr integration. SMM 02399–0136 has a corrected $450 \mu\text{m}$ flux density of 28 mJy , and so *FIRST* could typically detect about 120 sources comparable to SMM 02399–0136 at 5σ significance in each hour of integration. This tremendous haul would re-

quire careful ground-based follow-up observations in order to accurately locate and study the sources. Planned ground-based interferometer arrays (Brown 1996; Downes 1996) are expected to provide extremely high-resolution images with sub-arcsecond resolution in the mm/sub-mm. At $850\ \mu\text{m}$, such instruments should be capable of surveying of order $0.1\ \text{deg}^2$ to a 1σ sensitivity of $2\ \text{mJy}$ in a 1 hr integration (Blain 1996a). Hence, such a telescope could detect about 25 sources similar to SMM02399–0136 at 5σ significance in each hour of integration.

The future for sub-mm observations of active galaxies is clearly very bright because of the redshift-independent selection function in the sub-mm waveband and our tentative direct estimate of the abundance of obscured AGN. At the flux density limits discussed above, source confusion is not expected to be a problem in these observations (Blain, Ivison & Smail 1998). Even if the abundance of objects like SMM02399–0136 is an order of magnitude smaller than that suggested here, samples of many thousands of dust-shrouded AGN could still be compiled using *FIRST* and ground-based interferometer arrays, independent of the degree of intrinsic or line-of-sight extinction. The prospects for studying these objects using their mid-IR fine-structure line emission are also excellent (Loeb 1994; Blain 1996b; Stark 1997). These samples will allow the history of AGN activity at high redshifts to be studied in great detail.

5 CONCLUSIONS

(i) We have presented multi-wavelength observations of the first distant, sub-mm-selected, ultraluminous galaxy, SMM02399–0136, spanning the spectral regions from the radio to the X-ray.

(ii) Spectroscopy in the optical and near-IR wavebands indicate that the galaxy lies at $z = 2.80$ and consists of both a compact, dust-obscured AGN component, L1, and a companion source with more extended emission, L2. The emission line properties of L1 are very similar to those exhibited by F10214+4724. However, we show that the intrinsic bolometric luminosity of this galaxy is probably a factor of five times brighter than that of the *IRAS* source, F10214+4724.

(iii) The extended, weak radio emission from the galaxy is consistent with the sub-mm emission arising from *both* the compact and diffuse components, L1 and L2 respectively. Although we conclude that the emission from L1 arises either partly or wholly from a highly-obscured AGN, we ascribe the extended emission and structure visible in L2 to a very vigorous burst of star formation, probably triggered by an interaction involving L1 and L2.

(iv) At present, the detection of a single active galaxy in the sample of six sub-mm sources discovered by SIB does not compromise the conclusions of that paper. The predicted source counts and background radiation intensities are unaltered by finding a non-thermal contribution to the emission from SMM02399–0136; the density of metals at the present epoch, should be reduced by a factor of up to about 20 per cent, but remains in agreement with current observations.

(v) Based on these observations we estimate that the surface density of highly-obscured AGN, similar to SMM02399–0136, at $0.5 < z < 10$ is of order $250\ \text{deg}^{-2}$. If forthcoming SCUBA surveys confirm this abundance of

dust-shrouded AGN, then the proposed *FIRST* space mission and large ground-based interferometer arrays will provide potentially huge samples of dust-shrouded active galaxies.

(vi) We are currently undertaking a detailed study of the properties of the other sub-mm sources from the on-going SCUBA survey of SIB. The results from this will be presented in Ivison et al. (1998, in preparation).

ACKNOWLEDGEMENTS

RJI and IRS acknowledge the award of PPARC Advanced Fellowships. JPK acknowledges support from CNRS and from an ESEP (CNRS/RS) grant. We acknowledge useful conversations and help from Paul Alexander, Omar Almaini, Chris Done, K.S. Dwarakanath, Katherine Gunn, Andy Lawrence, Haida Liang, Richard McMahon, Leo Metcalfe, Tim Naylor, Frazer Owen, Max Pettini, Ian Robson and Tom Shanks.

REFERENCES

- Almaini O., Boyle B. J., Griffiths R. E., Shanks T., Stewart G. C., Georgantopoulos I., 1995, MNRAS, 277, L31
- Almaini O., Fabian A. C., Barcons X., 1998, MNRAS, in preparation
- Baldwin J. A., McMahon R., Hazard C., Williams R. E., 1988, ApJ, 327, 103
- Barbaro G., Poggianti B. M., 1997, A&A, 324, 490
- Barvainis R., Antonucci R., Hurt T., Coleman P., Reuter H.-P., 1995, ApJ, 451, L9
- Bershady M. A., et al., 1998, ApJ, in preparation
- Blain A. W., 1996a, in Shaver P. A. ed., Science with large millimetre arrays, Springer, Berlin, p. 70
- Blain A. W., 1996b, MNRAS, 283, 1340
- Blain A. W., 1997a, MNRAS, 290, 553
- Blain A. W., 1997b, in Wilson A., ed, The far-infrared and sub-millimetre universe, ESA vol. SP-401, ESA publications, Noordwijk, p. 175
- Blain A. W., Longair M. S., 1993, MNRAS, 264, 509
- Blain A. W., Longair M. S., 1996, MNRAS, 279, 847
- Blain A. W., Ivison R. J., Smail I., 1998, MNRAS, submitted; astro-ph/9710003
- Blain A. W., Smail I., Ivison R. J., 1998, MNRAS, in preparation
- Broadhurst T., Lehar J., 1995, ApJ, 450, L41
- Brown R., 1996, in Bremer M. N., van der Werf P. P., Röttgering H. J. A. eds, Cold gas at high redshifts, Kluwer, Dordrecht, p. 411
- Césarsky C. J. et al, 1996, A&A, 315, L32
- Couch W. J., Ellis R. S., Sharples R. M., Smail I., 1994, ApJ, 430, 121
- D’Oroico S., Goss W. M., Dopita M. A., 1982, MNRAS, 198, 1059
- Downes D., 1996, in Shaver P. A. ed., Science with large millimetre arrays, Springer, Berlin, p. 16
- Dunlop J. S., Hughes D. H., Rawlings S., Eales S. A., Ward M. J., 1994, Nat, 370, 347
- Eisenhardt P. R., Armus L., Hogg D. W., Soifer B. T., Neugebauer G., Werner M. W., 1996, ApJ, 461, 72
- Georgantopoulos I., Stewart G. C., Shanks T., Boyle B. J., Griffiths R. E., 1996, MNRAS, 280, 276
- Goodrich R. W., Miller J. S., Martel A., Cohen M. H., Tran H. D., Ogle P. M., Vermeulen R. C., 1996, ApJ, 456, L9
- Hartig G. F., Baldwin J. A., 1986, ApJ, 302, 64
- Heckman T. M., et al., 1995, ApJ, 452, 549

- Helou G., Soifer B. T., Rowan-Robinson M., 1985, *ApJ*, 298, L7
- Hill R. S., Home A. T., Smith A. M., Bruhweiler F. C., Cheng K. P., Hintzen P. M. N., Oliverson R. J., 1994, *ApJ*, 430, 568
- Holtzman J. A., Burrows C. J., Casterno S., Hester J. J., Trauger J. T., Watson A. M., Worthey G., 1995, *PASP*, 107, 1065
- Hutchings J. B., 1995, *AJ*, 110, 994
- Isaak K. G., McMahon R. G., Hills R. E., Withington S., 1994, *MNRAS*, 269, L28
- Ivison R. J., Archibald E. N., Dey A., Graham J. R., 1997, in Wilson A., ed, *The far-infrared and submillimetre universe*, ESA vol. SP-401, ESA publications, Noordwijk, p. 281
- Ivison R. J. et al., 1998, *ApJ*, in press; astro-ph/9709124
- de Jong T., Klein U., Wielebinski R., Wunderlich E., 1985, *A&A*, 147, L6
- Kennicutt R. C. Jr, 1983, *ApJ*, 272, 54
- Kneib J.-P., Mellier Y., Fort B., Mathez G., 1993, *A&A*, 273, 367
- Kneib J.-P., Mathez G., Fort B., Mellier Y., Soucail G., Longaretti P.-Y., 1994, 286, 701
- Lawrence A., Rigopoulou D., Rowan-Robinson M., McMahon R. G., Broadhurst T., Lonsdale C. J., 1994, *MNRAS*, 266, L41
- Lehnert M. D., Becker R. H., 1998, *A&A*, in press; astro-ph/9711113
- Liang H., 1997, PhD thesis, Australian National University
- Loeb A., 1993, *ApJ*, 404, L37
- Metcalfe L. et al., 1998, *A&A*, in preparation
- Ohta K., Yamada T., Nakanishi K., Ogasaka Y., Kii T., Hayashida K., 1996, *ApJ*, 458, L59
- Oke J. B., 1990, *AJ*, 99, 1621
- Oort M. J. A., 1987, *A&AS*, 71, 221
- Pearson C., Rowan-Robinson M., 1996, 283, 174
- Pilbratt G., 1997, in Wilson A. ed, *The far-infrared and submillimetre universe*, ESA vol. SP-401, ESA publications, Noordwijk, p. 7
- Phillips T. R., 1997, in Wilson A. ed, *The far-infrared and submillimetre universe*, ESA vol. SP-401, ESA publications, Noordwijk, p. 223
- Rowan-Robinson M. et al., 1991, *Nat*, 351, 719
- Rowan-Robinson M. et al., 1993, *MNRAS*, 261, 513
- Saunders W. S., Rowan-Robinson M., Lawrence A., Efstathiou G., Kaiser N., Ellis R. S., Frenk C. S., 1990, *MNRAS*, 248, 318
- Serjeant, S., Rawlings, S., Lacy, M., McMahon, R., Lawrence, A., Rowan-Robinson, M., Mountain, M., 1998, pre-print
- Smail I., Ellis R. S., Fitchett M. J., Nørgaard-Nielsen H. U., Hansen L., Jørgensen H. E., 1991, *MNRAS*, 252, 19
- Smail I., Ivison R. J., Blain A. W., 1997, *ApJ*, 490, L5 (SIB)
- Soucail G., Fort B., Mellier Y., Picat J. P., 1987, *A&A*, 172, L14
- Stark A. A., 1997, *ApJ*, 481, 587
- Thronson H., Telesco C., 1986, *ApJ*, 311, 98
- Wilner D. J., Wright M. C. H., 1997, *ApJ*, 488, L67
- Windhorst R. A., van Heerde G. M., Katgert P., 1984, *A&AS*, 58, 1